Published as: *Structure*. 2009 March 11; 17(3): 460–471.

# Cryoelectron tomography of homophilic adhesion mediated by the neural cell adhesion molecule L1

**Yongning He**[1], **Grant J. Jensen**[1], and **Pamela J. Bjorkman**[1,2,*]

[1] Division of Biology 114-96, California Institute of Technology, 1200 East California Blvd., Pasadena, CA 91125

[2] Howard Hughes Medical Institute, California Institute of Technology, 1200 East California Blvd., Pasadena, CA 91125

## Abstract

The neural cell adhesion molecule L1 participates in homophilic interactions that are important for axon guidance and neuronal development. The structural details of homophilic adhesion mediated by L1 and other immunoglobulin superfamily members containing an N-terminal horseshoe arrangement of four immunoglobulin-like domains are unknown. Here we used cryoelectron tomography to study liposomes to which intact or truncated forms of the L1 ectodomain were attached. Tomographic reconstructions revealed an adhesion interface with a regular and repeating pattern consistent with interactions between paired horseshoes contributed by L1 proteins from neighboring liposomes. The characteristics of the pattern, such as the space between horseshoe pairs and/or between adjacent membranes, changed when N-linked carbohydrates were altered by removing sialic acids or converting from complex to high mannose or oligomannose glycans, suggesting a regulatory role for carbohydrates in L1-mediated homophilic adhesion. Using the results from tomograms and crystal structures of L1-related molecules, we present a structural model for L1-mediated homophilic adhesion that depends on protein-protein, protein-carbohydrate, and carbohydrate-carbohydrate interactions.

The neural cell adhesion molecule L1 (CD171) is a cell surface protein expressed by predominantly neuronal, as well as some non-neuronal, cells in vertebrate and invertebrate species. L1 and related proteins function in neural development, axonal guidance, myelination, and cell migration by mediating both homophilic and heterophilic adhesion at the cell surface (Hortsch, 1996; Hortsch, 2000; Maness and Schachner, 2007). Heterophilic binding partners of L1 include other cell adhesion molecules, proteoglycans, extracellular matrix-associated molecules, integrins, receptor tyrosine phosphatases, and fibroblast growth factor receptor (Crossin and Krushel, 2000; Hortsch et al., 1998; Moos et al., 1988). Both homophilic and heterophilic interactions mediated by L1 are important in promoting or inhibiting neural outgrowth *in vivo* (Maness and Schachner, 2007).

L1 is a member of the immunoglobulin (Ig) gene superfamily, which includes other neural cell adhesion molecules such as neurofascin, NCAM, and TAG-1/axonin-1, all of which contain tandem Ig-like domains followed in some cases by fibronectin type III (FNIII) domains. L1 is composed of an ~1100 residue ectodomain containing six Ig-like domains followed by five

*Corresponding author: E-mail: bjorkman@caltech.edu, Phone: 626-395-8350, Fax: 626-792-3683.

FNIII repeats, a single-pass transmembrane region, and a 114-residue cytoplasm tail (Figure 1A) (Hortsch, 1996). Based on the crystal structures of two L1 homologues, hemolin (Su et al., 1998) and axonin-1 (Freigang et al., 2000), the four N-terminal Ig-like domains of L1 are predicted to adopt a horseshoe-shaped conformation in which the first and the second domains (D1 and D2) fold back to interact with the fourth and the third domains (D4 and D3), respectively (Figure 1A). The horseshoe conformation may be required for function, as the first four domains of L1 and related proteins are necessary and sufficient for homophilic adhesion (Haspel et al., 2000). The role of the FNIII domains in adhesion remains unclear, although some results suggest that they are involved in *cis*-interactions that facilitate heterophilic and/or homophilic interactions (Kunz et al., 2002).

The tandem arrangement of 11 consecutive domains in the L1 ectodomain suggests a flexible and extended structure. Indeed, electron microscopy (EM) studies of negatively-stained EM samples were consistent with an N-terminal horseshoe structure followed by a flexible extended region representing the remainder of the domains (Schurmann et al., 2001). Rotary-shadowed samples showed a more extended structure that did not include the N-terminal horseshoe, presumably because of interactions between the protein and the mica surface (Schurmann et al., 2001).

Like many surface adhesion proteins, human L1 is highly glycosylated, with 21 potential N-linked glycosylation sites in its ectodomain: four within the N-terminal horseshoe domains, five within the fifth and sixth Ig-like domains, and the remaining 12 sites in the FNIII domains. Carbohydrates have been shown to play a role in L1- and N-CAM-mediated neural adhesion (Acheson et al., 1991; Kadmon et al., 1990). In particular, L1 can bind to terminal sialic acids attached to complex carbohydrates, thereby acting as a sialic acid-binding lectin in regulating neurite growth (Crocker, 2002; Kleene et al., 2001).

Although X-ray and EM studies have provided some information about the structure of L1, a mechanistic understanding of homophilic adhesion mediated by membrane-bound L1 molecules and the roles of carbohydrates in adhesion remain to be clarified. Here we used cryoelectron tomography (cryoET) to investigate the three-dimensional structure of the homophilic adhesion interface formed between L1 molecules on opposing membranes. Our results suggest a new model for homophilic adhesion mediated by L1 family members in which horseshoes from proteins on opposing membranes meet as *trans* pairs, which form a regularly spaced lattice due to lateral contacts resulting from protein-carbohydrate and carbohydrate-carbohydrate interactions. Taken together with the demonstration that alterations in carbohydrate structure changed the structure of the adhesion interface, this model predicts a primary role for carbohydrates in regulating adhesion mediated by L1 and related proteins.

## RESULTS

### The L1 ectodomain and L1 Ig-like domains alone mediate homophilic adhesion

In order to prepare a model system in which the structural features of L1-mediated homophilic adhesion could be imaged by cryoET, we expressed His-tagged L1 proteins that could be attached to liposomes prepared from nickel-derivatized lipids. Since the cytoplasmic tail of L1 is not required for homophilic adhesion (Wong et al., 1995), we used recombinant proteins including all or part of the L1 ectodomain followed by a C-terminal His-tag, so that attachment to nickel lipids in a liposome would mimic the natural orientation on a cell membrane (Figure 1A). The proteins were expressed in mammalian (HEK293F) cells, which attach complex-type oligosaccharides with terminal sialic acids to N-linked glycosylation sites, and in insect (Hi5) cells, which attach smaller paucimannosidic or oligomannose structures to N-linked sites (Tomiya et al., 2003). Two recombinant proteins, $L1_{ecto}$, consisting of all 11 domains in the L1 ectodomain (6 Ig-like and 5 FNIII domains), and $Ig_{1–6}$, comprising the N-terminal Ig-like

domains only, were expressed in both systems, and named according to the nature of their N-linked glycans: $L1_{ecto\ (CC)}$, $Ig_{1–6\ (CC)}$, $L1_{ecto\ (OM)}$, and $Ig_{1–6\ (OM)}$ (where "CC" refers to complex carbohydrates produced in HEK293F cells and "OM" refers to oligomannose carbohydrates produced in Hi5 cells). In addition, $Ig_{1–4del\ (OM)}$, an L1 deletion mutant in which the four Ig-like domains involved in forming the N-terminal horseshoe were removed, was expressed in insect cells. As expected due to the larger size of complex versus oligomannose carbohydrates (Tomiya et al., 2003), SDS-PAGE analysis was consistent with higher molecular weights for $L1_{ecto\ (CC)}$ and $Ig_{1–6\ (CC)}$ compared with $L1_{ecto\ (OM)}$ and $Ig_{1–6\ (OM)}$ (Figure 1B).

We tested the ability of the L1 proteins to mediate homophilic adhesion by using light scattering to monitor liposome aggregation (Figure 2). In this assay, a His-tagged protein was added to nickel-derivatized liposomes, and the absorbance at 650 nm was monitored as a function of time. Addition of the mammalian and insect cell versions of $L1_{ecto}$ and $Ig_{1–6}$ resulted in increased light scattering compared to the background levels observed upon addition of $Ig_{1–4del\ (OM)}$, unrelated His-tagged control proteins, or buffer alone. These results demonstrated that the aggregation results were specific, as L1 proteins, but not unrelated His-tagged proteins or the $Ig_{1–4del\ (OM)}$ L1 protein, mediated adhesion when attached to liposomes. In addition, these results showed that the FNIII domains were not required for homophilic adhesion, since both the intact L1 ectodomain and the Ig-like domains of L1 alone mediated liposome aggregation.

## Structural features of L1-mediated homophilic revealed by cryoET

Frozen hydrated samples of liposomes aggregated by addition of L1 proteins were examined by cryoET (Supplementary Figure S1). Tomograms were calculated for liposomes prepared with insect cell-derived and mammalian cell-derived versions of $L1_{ecto}$ and $Ig_{1–6}$. In all cases, the tomograms showed clustered liposomes and occasional isolated liposomes. Most liposomes varied in diameter between 50 and 200 nm. Both leaflets of the membrane bilayer were usually distinguished in tomograms, although not always in individual 2D tomographic slices. Although most of the liposomes were unilamellar, some contained one or two inner vesicles. The multilamellar liposomes served as controls for identifying density due to attached L1 proteins because the His-tagged proteins had access to only the outermost membrane bilayer. L1 proteins attached to the liposome surface appeared as regions of higher density compared with the background. The higher density regions were most apparent at interfaces between clustered liposomes. We defined a homophilic interface as a contact area containing a region of higher contrast in the middle between two membranes. By this definition, we identified more than 50 individual interfaces in >20 tomograms. By contrast, liposomes prepared using $Ig_{1–4del}$ samples showed few clustered liposomes and no specific contact areas (Supplementary Figure S2).

Clustered liposomes showed regions separated by characteristic membrane-to-membrane distances and both elongated and punctuated densities between the adjacent membranes (Figure 3,4). For both the insect cell- and mammalian cell-produced proteins, the inter-membrane spacing at adhesion sites was usually larger for the $L1_{ecto}$ liposomes than for the $Ig_{1–6}$ liposomes: 190±22 Å for $L1_{ecto\ (OM)}$ compared with 160±20 Å for $Ig_{1–6\ (OM)}$, and 290±21 Å for $L1_{ecto\ (CC)}$ compared with 250±16 Å for $Ig_{1–6\ (CC)}$ (Figure 1D). In adhesion interfaces derived from liposomes produced with proteins expressed in insect cells, we found rows of regularly spaced "dots" of density parallel to the membrane planes in the middle of interface (Figure 3A,B and Supplementary Movie S1). In the samples involving mammalian cell-expressed proteins, the interfaces included elongated densities roughly perpendicular to the planes defined by the membranes in the adhesion interface in addition to dots in the middle of the interface (Figure 4A,B). The spacing between dots in the $L1_{ecto\ (OM)}$ and $Ig_{1–6(OM)}$ samples was ~140 Å, as compared to ~100 Å in the $L1_{ecto\ (CC)}$ and $Ig_{1–6(CC)}$ samples (Figure 1D). The

dots were larger (~70 Å diameter) and more distinct in the interfaces involving insect cell-derived proteins compared with proteins produced in mammalian cells (~60 Å diameter dots). In tomograms from the $L1_{ecto\ (OM)}$ and $Ig_{1–6\ (OM)}$ samples, we observed rows of up to 7–8 regularly spaced dots in some interfaces (more typically there were 2–5 dots per interface) and occasional two-dimensional ordered arrays of hexagonally-packed dots (Supplementary Figure S3). Examination of the tomograms revealed that many of the dot densities (at least half of ~100 observed dots) were distinctly U-shaped (Figure 3C), allowing the fitting of two horseshoes interacting in a similar manner as seen in the crystal structures of Dscam isoforms (Meijers et al., 2007) (Figure 3D,E and Supplementary Movies S2,S3). The same arrangement of horseshoe pairs also fit the more spherical dot densities derived from the $L1_{ecto\ (CC)}$ and $Ig_{1–6\ (CC)}$ samples (Figure 4C,D and Supplementary Movie S4).

## Alteration of L1 homophilic interfaces by carbohydrate modifications

Although we observed adhesion interfaces between liposomes prepared with both mammalian cell-derived and insect cell-derived L1 proteins, the structural details of the interfaces differed (Figure 1D, 3,4). N-terminal sequencing revealed that the hydrophobic leader peptides were cleaved at the same position in proteins produced in both systems (data not shown), and analogous constructs terminated at the same residue (Experimental Procedures), thus the protein portions of the molecules were the same. Instead of protein differences, we hypothesized that differences in N-linked carbohydrates attached to the mammalian cell- and insect cell-produced L1 proteins affected the structures of the resulting homophilic interfaces. To investigate this possibility, we used drug and enzymatic treatments to alter the carbohydrates attached to the mammalian cell-produced proteins. HEK293F cells were treated with kifunensine, a mannosidase inhibitor that results in attachment of relatively small high mannose ($Man_9(Glc_2Nac)_2$) sugars (Elbein et al., 1990) (Figure 1D), as compared with larger complex carbohydrates, to N-linked glycosylation sites. The resulting proteins, $L1_{ecto\ (CC\text{-}kif)}$ and $Ig_{1–6\ (CC\text{-}kif)}$, showed altered mobilities by SDS-PAGE and denaturing isoelectric focusing (Figure 1B.C). The mass spectroscopy-derived molecular weight for $Ig_{1–6\ (CC\text{-}kif)}$ was ~85 kD, as compared with ~90 kD for $Ig_{1–6\ (CC)}$ and ~81 kD for $Ig_{1–6\ (OM)}$, thus the high mannose carbohydrates resulting from kifunensine treatment of mammalian cells differed from the oligomannose glycans attached to N-linked sites on proteins produced in insect cells (Tomiya et al., 2003) (Figure 1D). We also treated purified $L1_{ecto\ (CC)}$ and $Ig_{1–6\ (CC)}$ proteins with sialidase to remove terminal sialic acids from the complex N-linked glycans. The resulting proteins, $L1_{ecto\ (CC\text{-}sial)}$ and $Ig_{1–6\ (CC\text{-}sial)}$, showed no reduction in apparent molecular mass by SDS-PAGE (data not shown), but analysis by denaturing isoelectric focusing demonstrated a shift to a more basic pI, consistent with removal of negatively-charged sialic acids (Figure 1C). All of the carbohydrate-modified proteins mediated liposome aggregation to the same extent as their untreated counterparts (Figure 2).

The adhesion interfaces in tomograms derived from both the kifunensine and sialidase-treated samples revealed some of the same general features previously observed for the samples with unaltered complex carbohydrates. However, the regularity of the interface density was largely lost, with fewer regularly spaced dots appearing at the interfaces of $L1_{ecto\ (CC\text{-}kif)}$ and $Ig_{1–6\ (CC\text{-}kif)}$ liposomes (Figure 5). The distance between clustered liposomes in the kifunensine- and sialidase-treated samples was generally smaller than their untreated counterparts: 260±36 Å and 250±34 Å for the $L1_{ecto\ (CC\text{-}kif)}$ and $L1_{ecto\ (CC\text{-}sial)}$ samples, respectively, and 200±22 Å for the $Ig_{1–6\ (CC\text{-}sial)}$ sample (Figure 1D). Only the $Ig_{1–6\ (CC\text{-}kif)}$ sample showed a similar separation distance as its untreated counterpart.

To investigate the potential for positively-charged residues on L1 to interact with negatively-charged sialic acids, we used HEK293F cells to express an L1 mutant (Arg184 to glutamine), which has been reported to lead to loss of function *in vitro* (Zhao et al., 1998) and neurological

disorders *in vivo* (De Angelis et al., 2002). The resulting protein, L1-R184Q$_{ecto\ (CC)}$, migrated similarly to L1$_{ecto\ (CC)}$ on SDS-PAGE and mediated homophilic adhesion in the liposome aggregation assay to the same degree as the L1$_{ecto}$ and Ig$_{1–6}$ proteins (data not shown). Analysis of the adhesion interfaces derived from L1-R184Q$_{ecto\ (CC)}$-coupled liposomes revealed similar intermembrane and inter-dot distances as the L1$_{ecto\ (CC)}$ samples (270±27 Å and ~100 Å for the intermembrane and inter-dot distances, respectively, of the L1-R184Q$_{ecto\ (CC)}$ samples) (Figure 1D). However, the L1-R184Q$_{ecto\ (CC)}$ adhesion interfaces differed from L1$_{ecto\ (CC)}$ interfaces in containing less regular density; i.e., regularly-spaced dots at the middle of the interfaces were less frequently observed (~80% of L1$_{ecto\ (CC)}$ interfaces contained regularly-spaced dots, compared with ~30% of L1-R184Q$_{ecto\ (CC)}$ interfaces). When dots were present in the L1-R184Q$_{ecto\ (CC)}$ interfaces, there were fewer connections between the dots and the membrane (Figure 5I,J).

## DISCUSSION

At the leading edge of a growth cone, L1 proteins interact homophilically with partners on adjacent membranes, a dynamic process involving endocytosis and recycling that requires both outside-in and inside-out signaling (Kamiguchi and Lemmon, 2000a; Kamiguchi and Lemmon, 2000b). Homophilic binding by L1 initiates outside-in signaling by recruiting ankyrin, a protein that associates with the actin-spectrin cytoskeleton (Bennett and Chen, 2001), to the adhesion site via binding to a conserved ankyrin binding sequence in the L1 cytoplasmic tail (Hortsch et al., 1998; Malhotra et al., 1998; Nagaraj and Hortsch, 2006). L1 homophilic adhesion also triggers transient dephosphorylation of a YRSLE motif in the L1 cytoplasmic domain, resulting in endocytosis (Nagaraj and Hortsch, 2006; Schaefer et al., 2002). A simple strategy for L1, a monomeric protein with a single-pass transmembrane helix, to signal to the inside of the cell that homophilic binding is taking place at the outside of the cell is to form clusters at adhesion sites (Kamiguchi and Lemmon, 2000a), thus bringing the L1 cytoplasmic tails close enough to allow ankyrin recruitment or dephosphorylation. Indeed, antibody-induced crosslinking of L1 in the absence of homophilic binding induces dephosphorylation of the cytoplasmic tail (Schaefer et al., 2002). This implies that lateral interactions between L1 proteins at an adhesion interface act as important structural cues for outside-in signaling. Here we used cryoET to investigate the structure of the L1 homophilic interface, finding a regular pattern of lateral interactions that changed upon alteration of N-linked carbohydrates.

We used a model system involving attachment of His-tagged L1 proteins to nickel-derivatized liposomes in order to form homophilic interfaces. The smaller size of liposomes as compared with cells allowed us to form interfaces in thin layers of ice that could be studied by cryoET without sectioning. A light scattering assay showed that the liposomes adhered to each other when L1 proteins, but not unrelated control proteins, were attached to the liposomes. Correlating with previous results (Haspel et al., 2000), we observed no adhesion in either the light scattering assay or by cryoET using Ig$_{1–4del\ (OM)}$, an L1 protein lacking the four Ig-like domains that form the N-terminal horseshoe structure. However, we observed homophilic adhesion using both the intact L1 ectodomain (L1$_{ecto}$; six N-terminal Ig-like domains followed by five FNIII domains) and using an L1 protein containing the Ig-like domains alone (Ig$_{1–6}$). These results are compatible with previous studies showing that constructs containing only the Ig-like domains of L1 or its avian homolog Ng-CAM functioned in homophilic adhesion and neurite outgrowth (Haspel et al., 2000). Although they were not absolutely required, other studies suggested that the L1 FNIII domains facilitated L1 multimerization and heterophilic or homophilic adhesion (Hall et al., 2000; Silletti et al., 2000; Stallcup, 2000).

Here we generated tomograms of the interfaces between adhering liposomes, which revealed structural features of L1-mediated homophilic adhesion. The tomograms included diffuse densities across the adhesion interfaces, and stronger, regularly-spaced globular densities,

appearing as "dots" in a row at the center of the interface. These results are not consistent with models for homophilic adhesion that postulate continuous zipper-like interactions arising from translational symmetries that repeat indefinitely: e.g., a model in which domain-swapped horseshoes were proposed to multimerize at the adhesion interface (Su et al., 1998) (Figure 6A, right model), which would appear in tomograms as densities corresponding to individual horseshoes in a zig-zag, or a model in which individual horseshoes were proposed to interact in a continuous zipper (Freigang et al., 2000) (Figure 6B), which would appear in tomograms as a solid line of density at the center of the adhesion interface.

Instead of a continuous arrangement of interacting proteins, the existence of discrete and regularly spaced dots of density suggested that the interface was composed of molecules that met in *trans* as pairs at the interface center, each partner contributing one N-terminal 4-domain horseshoe to form an 8-domain unit composed of two interacting horseshoes (Figure 6C). Pairs of interacting horseshoes, rather than a continuous zipper interaction, have also been proposed to explain the homophilic recognition properties of individual isoforms of Dscam (Meijers et al., 2007). The crystal structures of two Dscam isoforms revealed U-shaped horseshoe pairs in which the two horseshoes were related by a two-fold symmetry axis. The horseshoe pairs formed by the two different isoforms showed common interactions involving their D2 and D3 domains, but differed in the arrangement of the "arms" of the U (Meijers et al., 2007). The sizes of the Dscam horseshoe pairs (measured as ~60 Å × 70 Å × 80 Å and ~60 Å × 60 Å × 100 Å in the pdb files 2v5r and 2v5s) were in the range of the dots observed in our tomograms. Indeed, many of the dots in tomograms derived from $L1_{ecto\ (OM)}$ and $Ig_{1–6\ (OM)}$ samples were U-shaped rather than spherical (Figure 3C). A Dscam horseshoe pair could be fit into the U-shaped densities if the angle of the "arms" of the U was changed (Figure 3D,E and Supplementary Movie S2), a modification that seemed reasonable given that this angle differed in the structures of two Dscam isoforms (Meijers et al., 2007). Although the resolution of the tomograms (~4–5 nm) was adequate to approximately place individual domains within density given the assumption of the Dscam horseshoe pair model, we could not resolve connections between domains, thus a domain-swapped dimer of horseshoes, as hypothesized in one of the models based on the structure of the L1-related protein hemolin (Su et al., 1998) (Figure 6A), would also be compatible with the U-shaped densities and a Dscam style of pairing. Consistent with the suggestion that a pairing of this type, either domain-swapped or not, accounts for L1-mediated homophilic recognition, many of the critical interactions for Dscam pairing involved D2 (Meijers et al., 2007), and L1 D2 has been shown to contain residues required for its activity (Kenwrick and Doherty, 1998; Zhao et al., 1998). In addition, when the four predicted N-linked glycosylation sites in the L1 horseshoe were mapped onto the structure of the Dscam horseshoe pair, the carbohydrates were predicted to face solvent rather than the opposing horseshoe (Figure 3D and Supplementary Movie S2), suggesting that L1 horseshoes could adopt this mode of interaction without interference from N-linked glycans. An alignment of the horseshoe domains from mammalian L1 proteins with known sequences (human, rat, mouse, monkey, cow) reveals that the four predicted N-linked glycosylation sites are conserved in all sequences and there are no additional predicted sites (data not shown).

Assuming that the primary unit of homophilic adhesion is a pair of L1 proteins interacting in *trans* via their horseshoe domains, the next issue to address was what would account for horseshoe pairs being separated from each other by a regular distance. The separation distances differed in tomograms derived from liposomes containing proteins produced in mammalian cells versus insect cell-derived proteins: adhesion interfaces derived from $L1_{ecto\ (CC)}$ and $Ig_{1–6\ (CC)}$ liposomes, which included complex N-linked carbohydrates with terminal sialic acids, showed dots separated by ~100 Å, whereas interfaces derived from the analogous insect cell-derived proteins containing oligomannose N-linked carbohydrates ($L1_{ecto\ (OM)}$ and $Ig_{1–6\ (OM)}$) revealed dots separated by ~140 Å (Figure 1D, 3E, 4C,D). As the analogous proteins produced in mammalian and insect cell cells had the same starting and ending residues (see

Experimental Procedures), the most likely explanation for the observed differences in adhesion interfaces was the nature of the carbohydrate attached to potential N-linked carbohydrate sites (nine within the six Ig-like domains and 12 in the five FNIII domains).

To test whether altering carbohydrates on an L1 protein could change its adhesion interface, we treated $L1_{ecto}$- and $Ig_{1–6}$-expressing mammalian cells with kifunensine, resulting in proteins ($L1_{ecto\ (CC\text{-}kif)}$ and $Ig_{1–6\ (CC\text{-}kif)}$) containing a high mannose form of N-linked carbohydrate that lacked terminal sialic acids (Elbein et al., 1990). We also used sialidase to remove only the terminal sialic acids from purified $L1_{ecto\ (CC)}$ and $Ig_{1\text{-}6\ (CC)}$ proteins to create $L1_{ecto\ (CC–sial)}$ and $Ig_{1–6\ (CC\text{-}sial)}$. Treatment with kifunensine or sialidase raised the pI of the proteins such that their migration on denaturing IEF gels was similar to their insect cell-derived counterparts (Figure 1C), which were unaffected by sialidase treatment (data not shown), consistent with reports that insect cell proteins do not include terminal sialic acids on their N-linked glycans (Marchal et al., 2001). The N-linked glycans resulting from either kifunensine or sialidase treatment of the mammalian cell-derived proteins differed from both their untreated counterparts and from the oligomannose structures attached by insect cells (Figure 1D). Accordingly, the interfaces of adhering liposomes produced using the kifunensine- or sialidase-treated $L1_{ecto}$ and $Ig_{1–6}$ samples revealed differences from liposomes produced using either the insect cell-derived or the untreated mammalian cell-derived proteins. For example, the inter-membrane distances at the interfaces became smaller (Figure 1D) and the pattern of dots at the center of the adhesion interface became less obvious (Figure 5). Taken together with the observed differences in tomograms between the $L1_{ecto\ (CC)}/Ig_{1\text{-}6\ (CC)}$ versus $L1_{ecto\ (OM)}/Ig_{1–6\ (OM)}$ samples, the kifunensine- and sialidase-induced differences in adhesion interefaces suggested that the composition of the N-linked carbohydrate, and in particular, the presence or absence of sialic acids on L1 N-linked glycans, affected the structure of homophilic interfaces mediated by L1.

Carbohydrate-mediated alterations in the structure of a homophilic interface is consistent with current ideas that protein-carbohydrate and carbohydrate-carbohydrate interactions affect adhesion (Bucior and Burger, 2004; Patel et al., 2007). For example, carbohydrates can modulate homophilic adhesion by Ig superfamily members such as L1, N-CAM (Acheson et al., 1991; Kadmon et al., 1990), and the coxsackie and adenovirus receptor (CAR) (Excoffon et al., 2007). In particular, terminal sialic acids on complex carbohydrates regulated adhesion functions of N-CAM (Fujimoto et al., 2001; Varki, 2007), and heterophilic recognition of CD24 by L1 (Kleene et al., 2001). In the case of the L1-CD24 interaction, recognition of CD24-associated sialic acids was hypothesized to involve a conserved sequence in the first FNIII domain of L1 (Kleene et al., 2001). However, an FNIII domain cannot be solely responsible for the effect of sialic acids in our experiments, because we observed sialic acid-dependent changes in homophilic interfaces using the $Ig_{1–6}$ samples, which did not contain FNIII domains. In addition, the lateral separation between adhesion dots was similar in the $L1_{ecto\ (CC)}$ and the $Ig_{1–6\ (CC)}$ samples, indicating that the FNIII domains were not required for the relevant carbohydrate-protein interactions. Thus the potential involvement of sialic acids in homophilic adhesion by L1 must, at least in part, involve its Ig-like domains.

Sialic acid recognition by Ig-like domains is well-documented in a family of sialic acid-binding lectins, the Siglecs, which are members of the Ig superfamily (Crocker, 2002). Crystallographic and sequence analyses suggest a common mode of recognition of sialic acids by Siglec domains, involving an ionic interaction between the sialic acid carboxylate group and the guanidino group of an arginine located on strand F of a Siglec Ig-like domain (Zaccai et al., 2007). Arginine residues in the D2 and D3 domains of the L1-related protein hemolin also mediate interactions with a negatively-charged binding partner (in this case, a phosphate ion thought to mimic lipopolysaccharide) (Su et al., 1998). One of these arginines, Arg153 in the hemolin D2 domain, is conserved in L1 and axonin-1 sequences (L1 Arg184), making it a

potential candidate for recognition of negatively-charged sialic acids. In the Dscam-based model for a pair of interacting L1 horseshoe domains, Arg184 is located on the outside of the D2 domains of a horsehoe pair, where it is in a position that would be accessible to sialic acids from a neighboring L1 protein (Figure 3D,E and Supplementary Movies S2, S3). Although mutation of L1 Arg184 to glutamine leads to neurological disorders *in vivo* (De Angelis et al., 2002), we found that an $L1_{ecto}$ version of this mutant expressed in mammalian cells ($L1\text{-}R184Q_{ecto\ (CC)}$) still mediated homophilic adhesion, and that most features of its adhesion interface were similar to those of wildtype L1 (Figure 1D, 4,5). However, the interface patterns formed by this mutant were consistently less regular than wildtype L1 interfaces, suggesting that the mutation has a subtle influence in lateral pattern formation that might affect normal adhesive function. Further studies will be required to determine the effects of this mutation on other L1 functions, including heterophilic adhesion, and to precisely map the L1 residues that mediate lateral interactions involving complex carbohydrates.

Combining observations derived from our tomography studies, we propose a structural model for homophilic adhesion mediated by L1. Figure 6C shows schematic models for adhesion interfaces predicted when L1 proteins contain complex carbohydrates (top) or oligomannose carbohydrates (bottom). In both cases, two horseshoes from L1 proteins on opposing membranes meet in *trans* as a homophilic binding pair, forming a two-fold symmetric pair of horseshoes that resembles homophilic interactions of Dscam isoforms (Meijers et al., 2007). Unlike previously-proposed models for L1-mediated adhesion (Freigang et al., 2000; Su et al., 1998) (Figure 6A,B), the primary adhesion unit in our model is a pair of L1 proteins rather than a repeating set of inter-membrane and lateral interactions with translational symmetry. We propose that lateral (*cis*) interactions result from protein-carbohydrate interactions (in the case of L1 proteins containing complex carbohydrates) or carbohydrate-carbohydrate interactions (in the case of L1 proteins containing uncharged oligomannose carbohydrates). Although both types of lateral interactions would create approximately regular intervals between the adhesion pairs, the separation distances are predicted to differ in the case of L1 proteins containing complex (top schematic in Figure 6C) versus oligomannose carbohydrates (bottom schematic in Figure 6C).

Carbohydrates can extend ~35 Å from the surface of a protein (Flint et al., 2005) (Figure 3D), thus accounting for part of the observed separation distances between horseshoe pairs (Figure 1D, 3,4). In situations in which N-linked carbohydrates contain terminal sialic acids, recognition of the sialic acid on a neighboring L1 molecule would contribute to attractive forces between L1 neighbors, decreasing the average lateral separation. Accordingly, in the adhesion interfaces formed by the $L1_{ecto\ (CC)}$ and $Ig_{1–6\ (CC)}$ proteins, the average separation between adhesion pairs was ~100 Å, which can be accounted for by the diameter of an adhesion dot (~60–70 Å) plus a carbohydrate unit (~35 Å) that is making a carbohydrate-protein contact with a neighboring L1 protein (top schematic in Figure 6C). By contrast, the average dot separation was ~140 Å in the interfaces from oligomannose-containing samples in which sialic acids were not present ($L1_{ecto\ (OM)}$ and $Ig_{1–6\ (OM)}$), which can be accounted for by the diameter of an adhesion dot plus a “shield” or “halo” of carbohydrate units (Figure 3D) that would add another ~70 Å (bottom schematic in Figure 6C). In the oligomannose-containing samples, we speculate that the separation distance was determined by carbohydrate-carbohydrate interactions that form a “shield” around an L1 horseshoe pair, such that the pairs would space regularly at an adhesion interface even in the absence of forces that would impose translational or rotational symmetry.

Along with carbohydrate-induced changes in lateral spacing, we also observed changes in inter-membrane spacing, such that the sialyated samples generally showed larger separations. This could result from increased membrane repulsion, as observed for other adhesive interactions

involving sialyated proteins (Johnson et al., 2005), and/or carbohydrate-induced changes in the degree to which the L1 molecules were extended.

Thus in our model for L1-mediated homophilic adhesion, protein-protein interactions are responsible for *trans* interactions through pairing of horseshoe domains, and N-linked carbohydrates determine the *cis* spacing between adjacent L1 proteins on a membrane and influence the inter-membrane spacing. Given our evidence that N-linked carbohydrates play a critical role in determining the structure of the adhesion interface, we believe that not all physiologically-relevant interactions would be observed in structural studies involving protein produced in bacteria (Freigang et al., 2000). Our model predicts that carbohydrate-mediated changes in the pattern of lateral interactions could act as a regulating factor for downstream signaling pathways, and that lateral interactions of adhesion molecules could be important in setting the proper inter-membrane distance at adhesion sites, hence providing a scaffold for further receptor-ligand interactions between membranes.

## EXPERIMENTAL PROCEDURES

### Protein expression

The human L1 gene (kindly provided by Dr. Vance Lemmon, University of Miami) was amplified by PCR to make C-terminally His-tagged constructs encoding the L1 hydrophobic signal peptide (residues 1–19) and the ectodomain (residues 20–1119) (referred to as $L1_{ecto}$), or the signal peptide and the six Ig-like domains (residues 20–611) (referred to as $Ig_{1–6}$). The amplified products were subcloned into the pcDNA3.0 vector (Invitrogen), verified by sequencing, and then introduced into HEK293F cells by transient transfection using Lipofectamine (Invitrogen) following the manufacturer's protocol. To distinguish the resulting proteins from analogous versions with different carbohydrates, the proteins produced in HEK293F cells were named $L1_{ecto\ (CC)}$ and $Ig_{1–6\ (CC)}$, where "CC" refers to complex carbohydrates. Secreted $L1_{ecto\ (CC)}$ and $Ig_{1–6\ (CC)}$ proteins were purified from supernatants collected six days after transfection by sequential Ni-NTA affinity chromatography and gel filtration using a Superdex 200 column run in Tris-buffered saline (TBS; 50mM Tris pH 7.5, 150mM NaCl). The Arg184 to glutamine mutant of L1 (L1-R184$Q_{ecto\ (CC)}$) was prepared by site-directed mutagenesis of the wild-type L1 gene. The protein was expressed and purified from the supernatants of HEK293F cells as described above.

For some experiments, purified proteins produced in HEK293F cells were incubated with sialidase (Sigma) in 50 mM sodium phosphate, pH 5.0 for 5 hours at 37°C, and then buffer exchanged into TBS. Sialidase-treated proteins were referred to as $L1_{ecto\ (CC\text{-}sial)}$ and $Ig_{1–6\ (CC\text{-}sial)}$. In other experiments, transfected HEK293F cells were cultured with 15 ng/ml kifunensine (kif) (Toronto Research Chemical Inc.), a mannosidase I inhibitor that has been used to produce proteins in mammalian cells that contain high mannose, rather than complex, forms of N-linked oligosaccharides (Elbein et al., 1990). $L1_{ecto\ (CC\text{-}kif)}$ and $Ig_{1–6\ (CC\text{-}kif)}$ proteins were secreted from kifunensine-treated transfected HEK293F cells and purified as described for the proteins produced by untreated HEK293F cells.

Proteins with paucimannosidic or oligomannose (OM) N-linked carbohydrates were produced by expression in insect cells. $L1_{ecto\ (OM)}$, $Ig_{1–6\ (OM)}$, and $Ig_{1–4del\ (OM)}$, an L1 protein missing the four N-terminal horseshoe domains (constructed by fusing the cDNA encoding the L1 signal peptide to the cDNA encoding L1 residues 430–1119), were expressed as C-terminally 6x-His-tagged proteins in baculovirus-infected Hi5 cells. The L1 constructs were subcloned after sequencing into the pFASTBac vector (Invitrogen) and recombinant baculoviruses were generated as described by the manufacturer. Secreted 6x-His-tagged proteins were purified from the supernatants from infected Hi5 cells as described for the proteins expressed in mammalian cells.

### Protein characterization

$L1_{ecto\ (CC)}$, $L1_{ecto\ (OM)}$, $Ig_{1–6\ (CC)}$, and $Ig_{1–6\ (OM)}$ proteins were blotted to polyvinylidene difluoride (PVDF) membranes (Millipore) and N-terminal sequencing data were obtained on a Procise protein micro-sequencer (Applied Biosystems) at the Caltech Protein/Peptide Microanalytical Laboratory (PPMAL). In all cases, the sequence obtained was IQIPEEY, demonstrating that cleavage of the hydrophobic leader peptide occurred in the same position (after residue 19). Western blot analyses demonstrated that the soluble L1 proteins were recognized by a goat anti-human L1 polyclonal antibody (Santa Cruz Biotechnology) (data not shown). The approximate molecular weights of $Ig_{1–6\ (CC)}$, $Ig_{1–6\ (OM)}$, and $Ig_{1–6\ (CC\text{-}kif)}$ proteins were determined by matrix assisted, laser desorption, time-of-flight (MALDI-TOF) mass spectroscopy using a Voyager DC.str mass spectrometer (PerSeptive Biosystems, Inc.) at the Caltech PPMAL. The $L1_{ecto}$ proteins were too large for determining molecular weights by MALDI-TOF mass spectroscopy.

### Isoelectric focusing

Selected proteins were examined by denaturing isoelectric focusing (IEF) using 7.5% acrylamide gels containing 8M urea and 8.5% Bio-lyte 3/10 ampholytes (Bio-Rad). Gels were stained and destained with Biorad IEF gel staining and R-250 destain solutions, respectively. Standard proteins with known pI values were obtained from Biorad.

### Preparation of liposomes

Liposomes were prepared using nickel-derivatized lipids (1,2-Dioleoyl-*sn*-Glycero-3-[(N-(5-amino-1 carboxypentyl)iminodiacetic acid)succinyl] [Nickel salt]) (DOGS-NTA) (Avanti Lipids) by a standard hydration-extrusion method as described by the manufacturer. Briefly, 0.5 μmoles of DOGS-NTA in $CHCl_3$ were evaporated under nitrogen. The dry film was hydrated with 0.65 ml of TBS. After one hour of hydration, the mixture was passed through an Avanti Mini-Extruder using a 0.2 μm membrane.

### Liposome aggregation assay

Nickel-derivatized liposomes were incubated in TBS with 1 μM His-tagged L1 proteins, control His-tagged proteins [FcRY (West et al., 2004), M155 and MULT-1 (gifts of Z. Yang)], or buffer alone. Aggregation of liposomes was followed by monitoring the light scattering at 650 nm as a function of time in a Beckman DU-64 spectrophotometer. Readings were taken at time zero and then every five minutes for 40 minutes after adding a His-tagged protein or buffer control.

### Electron cryotomography

Aggregated liposomes were mixed with 10 nm colloidal gold particles (BB International) to serve as fiducial markers during image alignment procedures. Samples were loaded onto glow-discharged lacy carbon grids (Ted Pella, Inc.) and vitrified in liquid ethane using a Vitrobot (FEI). Liposome aggregates were identified as regions of darker contrast in thin ice. Tilt series (±60°, 1.5° angular increments) were digitally recorded on the GIF CCD using the UCSF tomography software package (Zheng et al., 2007) on a 300 kV, FEG, G2 Polara transmission EM (FEI). Images were acquired under low-dose conditions (80–100$e^{-}/Å^2$ total for the tilt series) 6–8 μm underfocus (first CTF zero at 3.5 – 4.0 nm) at 34,000x such that each pixel represented 6.8 Å. In some cases, dual-axis tilt series were recorded by rotating the grid 90° (Iancu et al., 2005).

### 3D reconstructions and image analysis

Tomographic reconstructions were calculated using the IMOD software package (Kremer et al., 1996; Mastronarde, 1997) for each tilt series using 10 nm gold particles as fiducial markers. For dual-axis tilt series, the resulting tomograms were aligned to each other and combined using IMOD. Areas of interest (adhering liposomes) were selected manually in the tomograms. The tomograms were not denoised because the major structural features of L1-mediated homophilic adhesion could be recognized without denoising. The programs O (Jones, 1990) and Chimera (Goddard et al., 2007) were used for visualizing small volumes of the 3D maps and for fitting crystal structures. Supplemental movies S1–S4 were made using Chimera.

The crystal structures of two Dscam adhesion pairs (PDB codes 2v5r and 2v5m) were manually fit into "U-shaped" dot densities after adjusting the angle between the two horseshoe-shaped molecules in each pair, which differed between the two pairs of Dscam isoforms (Meijers et al., 2007), while maintaining the adhesion interface around domains D2 and D3. Slightly different adjustments in this angle were required for fitting different dots. In order to locate potential N-linked glycosylation sites and L1 residue Arg184 on the horsehoe pairs, the coordinates of the horseshoe domains from the closest L1 relative with a known structure (axonin-1; pdb code 1cs6; 28% amino acid identity with L1) were superimposed on the Dscam domains, and analogous positions for the residues of interest were identified in the Dscam/axonin-1 model. An atomic model of an N-linked glycan constructed using carbohydrates from pdb code 1w8t (Flint et al., 2005) was attached to the approximate positions of the four potential N-linked glycosylation sites in each L1 horseshoe, creating eight N-linked glycans per horseshoe pair.

## Supplementary Material

Refer to Web version on PubMed Central for supplementary material.

## Acknowledgments

We thank Jost Vielmetter, Inderjit Nangiana, Chris Foglesong and the Caltech Protein Expression Center for expression of proteins, William Tivol and Prabha Dias for help with microscopy, and members of the Bjorkman and Jensen laboratories for helpful suggestions. Mass spectroscopic analysis and N-terminal sequencing performed by the Protein/Peptide Microanalytical Laboratory was supported by The Beckman Institute at Caltech. This work was supported by a postdoctoral fellowship from the Cancer Research Institute (Y.H.), the Howard Hughes Medical Institute (P.J.B.), and gifts to Caltech to support electron microscopy from the Gordon and Betty Moore Foundation and the Agouron Institute.

## References

Acheson A, Sunshine JL, Rutishauser U. NCAM polysialic acid can regulate both cell-cell and cell-substrate interactions. J Cell Biol 1991;114:143–153. [PubMed: 2050739]

Bennett V, Chen L. Ankyrins and cellular targeting of diverse membrane proteins to physiological sites. Curr Opin Cell Biol 2001;13:61–67. [PubMed: 11163135]

Bucior I, Burger MM. Carbohydrate-carbohydrate interactions in cell recognition. Curr Opin Struct Biol 2004;14:631–637. [PubMed: 15465325]

Crocker PR. Siglecs: sialic-acid-binding immunoglobulin-like lectins in cell-cell interactions and signalling. Curr Opin Struct Biol 2002;12:609–615. [PubMed: 12464312]

Crossin KL, Krushel LA. Cellular signaling by neural cell adhesion molecules of the immunoglobulin superfamily. Dev Dyn 2000;218:260–279. [PubMed: 10842356]

De Angelis E, Watkins A, Schafer M, Brummendorf T, Kenwrick S. Disease-associated mutations in L1 CAM interfere with ligand interactions and cell-surface expression. Hum Mol Genet 2002;11:1–12. [PubMed: 11772994]

Elbein AD, Tropea JE, Mitchell M, Kaushal GP. Kifunensine, a potent inhibitor of the glycoprotein processing mannosidase I. J Biol Chem 1990;265:15599–15605. [PubMed: 2144287]

Excoffon KJ, Gansemer N, Traver G, Zabner J. Functional effects of coxsackievirus and adenovirus receptor glycosylation on homophilic adhesion and adenoviral infection. J Virol 2007;81:5573–5578. [PubMed: 17376928]

Flint J, Bolam DN, Nurizzo D, Taylor EJ, Williamson MP, Walters C, Davies GJ, Gilbert HJ. Probing the mechanism of ligand recognition in family 29 carbohydrate-binding modules. J Biol Chem 2005;280:23718–23726. [PubMed: 15784618]

Freigang J, Proba K, Leder L, Diederichs K, Sonderegger P, Welte W. The crystal structure of the ligand binding module of axonin-1/TAG-1 suggests a zipper mechanism for neural cell adhesion. Cell 2000;101:425–433. [PubMed: 10830169]

Fujimoto I, Bruses JL, Rutishauser U. Regulation of cell adhesion by polysialic acid. Effects on cadherin, immunoglobulin cell adhesion molecule, and integrin function and independence from neural cell adhesion molecule binding or signaling activity. J Biol Chem 2001;276:31745–31751. [PubMed: 11425861]

Goddard TD, Huang CC, Ferrin TE. Visualizing density maps with UCSF Chimera. J Struct Biol 2007;157:281–287. [PubMed: 16963278]

Hall H, Bozic D, Fauser C, Engel J. Trimerization of cell adhesion molecule L1 mimics clustered L1 expression on the cell surface: influence on L1-ligand interactions and on promotion of neurite outgrowth. J Neurochem 2000;75:336–346. [PubMed: 10854279]

Haspel J, Friedlander DR, Ivgy-May N, Chickramane S, Roonprapunt C, Chen S, Schachner M, Grumet M. Critical and optimal Ig domains for promotion of neurite outgrowth by L1/Ng-CAM. J Neurobiol 2000;42:287–302. [PubMed: 10645969]

Hortsch M. The L1 family of neural cell adhesion molecules: old proteins performing new tricks. Neuron 1996;17:587–593. [PubMed: 8893017]

Hortsch M. Structural and functional evolution of the L1 family: are four adhesion molecules better than one? Mol Cell Neurosci 2000;15:1–10. [PubMed: 10662501]

Hortsch M, Homer D, Malhotra JD, Chang S, Frankel J, Jefford G, Dubreuil RR. Structural requirements for outside-in and inside-out signaling by Drosophila neuroglian, a member of the L1 family of cell adhesion molecules. J Cell Biol 1998;142:251–261. [PubMed: 9660878]

Iancu CV, Wright ER, Benjamin J, Tivol WF, Dias DP, Murphy GE, Morrison RC, Heymann JB, Jensen GJ. A “flip-flop” rotation stage for routine dual-axis electron cryotomography. J Struct Biol 2005;151:288–297. [PubMed: 16129619]

Johnson CP, Fujimoto I, Rutishauser U, Leckband DE. Direct evidence that neural cell adhesion molecule (NCAM) polysialylation increases intermembrane repulsion and abrogates adhesion. J Biol Chem 2005;280:137–145. [PubMed: 15504723]

Jones, TA.; Bergdoll, M.; Kjeldgaard, M. Crystallographic and Modeling Methods in Molecular Design. Springer-Verlag Press; 1990. A macromolecular modeling environment.

Kadmon G, Kowitz A, Altevogt P, Schachner M. Functional cooperation between the neural adhesion molecules L1 and N-CAM is carbohydrate dependent. J Cell Biol 1990;110:209–218. [PubMed: 2295683]

Kamiguchi H, Lemmon V. IgCAMs: bidirectional signals underlying neurite growth. Curr Opin Cell Biol 2000a;12:598–605. [PubMed: 10978896]

Kamiguchi H, Lemmon V. Recycling of the cell adhesion molecule L1 in axonal growth cones. J Neurosci 2000b;20:3676–3686. [PubMed: 10804209]

Kenwrick S, Doherty P. Neural cell adhesion molecule L1: relating disease to function. Bioessays 1998;20:668–675. [PubMed: 9780841]

Kleene R, Yang H, Kutsche M, Schachner M. The neural recognition molecule L1 is a sialic acid-binding lectin for CD24, which induces promotion and inhibition of neurite outgrowth. J Biol Chem 2001;276:21656–21663. [PubMed: 11283023]

Kremer JR, Mastronarde DN, McIntosh JR. Computer visualization of three-dimensional image data using IMOD. J Struct Biol 1996;116:71–76. [PubMed: 8742726]

Kunz B, Lierheimer R, Rader C, Spirig M, Ziegler U, Sonderegger P. Axonin-1/TAG-1 mediates cell-cell adhesion by a cis-assisted trans-interaction. J Biol Chem 2002;277:4551–4557. [PubMed: 11733523]

Malhotra JD, Tsiotra P, Karagogeos D, Hortsch M. Cis-activation of L1-mediated ankyrin recruitment by TAG-1 homophilic cell adhesion. J Biol Chem 1998;273:33354–33359. [PubMed: 9837910]

Maness PF, Schachner M. Neural recognition molecules of the immunoglobulin superfamily: signaling transducers of axon guidance and neuronal migration. Nat Neurosci 2007;10:19–26. [PubMed: 17189949]

Marchal I, Jarvis DL, Cacan R, Verbert A. Glycoproteins from insect cells: sialylated or not? Biol Chem 2001;382:151–159. [PubMed: 11308014]

Mastronarde DN. Dual-axis tomography: an approach with alignment methods that preserve resolution. J Struct Biol 1997;120:343–352. [PubMed: 9441937]

Meijers R, Puettmann-Holgado R, Skiniotis G, Liu JH, Walz T, Wang JH, Schmucker D. Structural basis of Dscam isoform specificity. Nature 2007;449:487–491. [PubMed: 17721508]

Moos M, Tacke R, Scherer H, Teplow D, Fruh K, Schachner M. Neural adhesion molecule L1 as a member of the immunoglobulin superfamily with binding domains similar to fibronectin. Nature 1988;334:701–703. [PubMed: 3412448]

Nagaraj K, Hortsch M. Phosphorylation of L1-type cell-adhesion molecules--ankyrins away! Trends Biochem Sci 2006;31:544–546. [PubMed: 16904324]

Patel TR, Harding SE, Ebringerova A, Deszczynski M, Hromadkova Z, Togola A, Paulsen BS, Morris GA, Rowe AJ. Weak self-association in a carbohydrate system. Biophys J 2007;93:741–749. [PubMed: 17483161]

Schaefer AW, Kamei Y, Kamiguchi H, Wong EV, Rapoport I, Kirchhausen T, Beach CM, Landreth G, Lemmon SK, Lemmon V. L1 endocytosis is controlled by a phosphorylation-dephosphorylation cycle stimulated by outside-in signaling by L1. J Cell Biol 2002;157:1223–1232. [PubMed: 12082080]

Schurmann G, Haspel J, Grumet M, Erickson HP. Cell adhesion molecule L1 in folded (horseshoe) and extended conformations. Mol Biol Cell 2001;12:1765–1773. [PubMed: 11408583]

Silletti S, Mei F, Sheppard D, Montgomery AM. Plasmin-sensitive dibasic sequences in the third fibronectin-like domain of L1-cell adhesion molecule (CAM) facilitate homomultimerization and concomitant integrin recruitment. J Cell Biol 2000;149:1485–1502. [PubMed: 10871287]

Stallcup WB. The third fibronectin type III repeat is required for L1 to serve as an optimal substratum for neurite extension. J Neurosci Res 2000;61:33–43. [PubMed: 10861797]

Su XD, Gastinel LN, Vaughn DE, Faye I, Poon P, Bjorkman PJ. Crystal structure of hemolin: a horseshoe shape with implications for homophilic adhesion. Science 1998;281:991–995. [PubMed: 9703515]

Tomiya N, Betenbaugh MJ, Lee YC. Humanization of lepidopteran insect-cell-produced glycoproteins. Acc Chem Res 2003;36:613–620. [PubMed: 12924958]

Varki A. Glycan-based interactions involving vertebrate sialic-acid-recognizing proteins. Nature 2007;446:1023–1029. [PubMed: 17460663]

West AP Jr, Herr AB, Bjorkman PJ. The chicken yolk sac IgY receptor, a functional equivalent of the mammalian MHC-related Fc receptor, is a phospholipase A2 receptor homolog. Immunity 2004;20:601–610. [PubMed: 15142528]

Wong EV, Cheng G, Payne HR, Lemmon V. The cytoplasmic domain of the cell adhesion molecule L1 is not required for homophilic adhesion. Neurosci Lett 1995;200:155–158. [PubMed: 9064600]

Zaccai NR, May AP, Robinson RC, Burtnick LD, Crocker PR, Brossmer R, Kelm S, Jones EY. Crystallographic and in silico analysis of the sialoside-binding characteristics of the Siglec sialoadhesin. J Mol Biol 2007;365:1469–1479. [PubMed: 17137591]

Zhao X, Yip PM, Siu CH. Identification of a homophilic binding site in immunoglobulin-like domain 2 of the cell adhesion molecule L1. J Neurochem 1998;71:960–971. [PubMed: 9721721]

Zheng SQ, Keszthelyi B, Branlund E, Lyle JM, Braunfeld MB, Sedat JW, Agard DA. UCSF tomography: an integrated software suite for real-time electron microscopic tomographic data collection, alignment, and reconstruction. J Struct Biol 2007;157:138–147. [PubMed: 16904341]

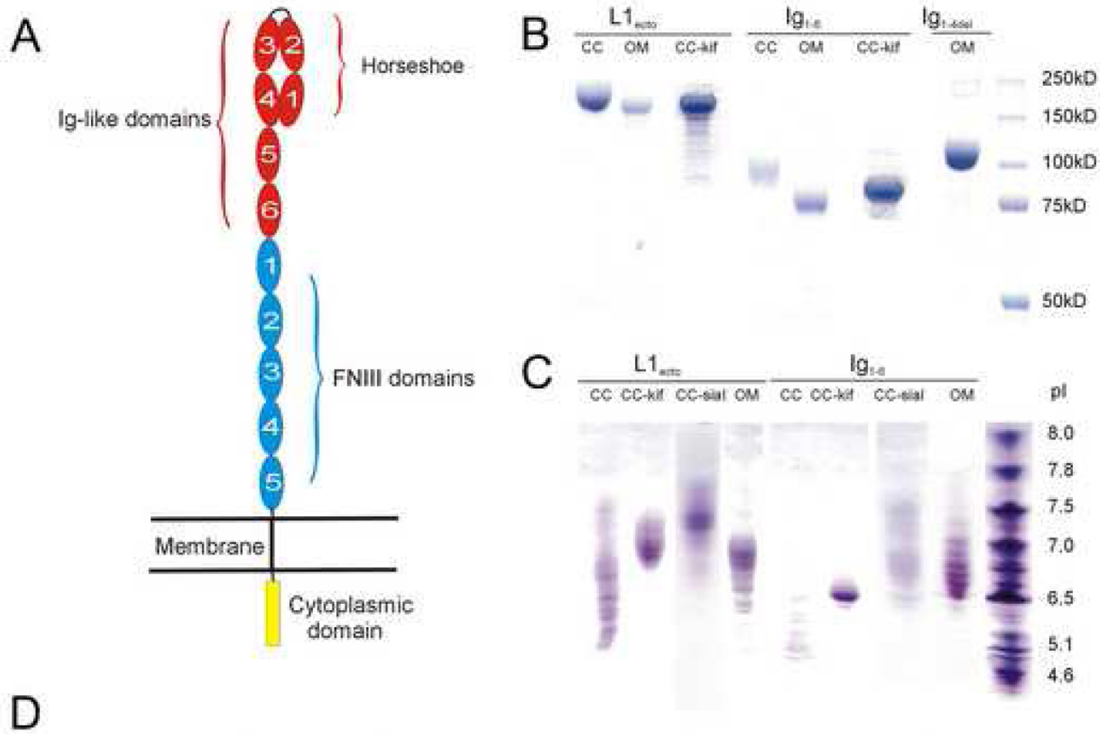


D

| Molecule | No. N-linked sites | Structure | Membrane distance (Å) | Dot distance (Å) |
|---|---|---|---|---|
| $L1_{ecto\ (CC)}$ | 21 | $(Neu5Ac\text{-}Gal\text{-}GlcNAc\text{-}Man)_2ManGlcNAc_2$ | 290±21; n=22 (250-380) | ~100 |
| $L1_{ecto\ (OM)}$ | 21 | $Man_{3-4}GlcNAc_2$ | 190±22; n=27 (160-240) | ~140 |
| $L1_{ecto\ (CC\text{-}kif)}$ | 21 | $Man_5GlcNAc_2$ | 260±36; n=14 (210-320) | - |
| $L1_{ecto\ (CC\text{-}sial)}$ | 21 | $(Gal\text{-}GlcNAc\text{-}Man)_2ManGlcNAc_2$ | 250±34; n=20 (200-320) | - |
| $L1\text{-}R184Q_{ecto\ (CC)}$ | 21 | $(Neu5Ac\text{-}Gal\text{-}GlcNAc\text{-}Man)_2ManGlcNAc_2$ | 270±27; n=24 (230-340) | ~100 |
| | | | | |
| $Ig_{1\text{-}6\ (CC)}$ | 9 | $(Neu5Ac\text{-}Gal\text{-}GlcNAc\text{-}Man)_2ManGlcNAc_2$ | 250±16; n=12 (230-270) | ~100 |
| $Ig_{1\text{-}6\ (OM)}$ | 9 | $Man_{3-4}GlcNAc_2$ | 160±20; n=12 (150-220) | ~140 |
| $Ig_{1\text{-}6\ (CC\text{-}kif)}$ | 9 | $Man_5GlcNAc_2$ | 250±13; n=11 (230-270) | - |
| $Ig_{1\text{-}6\ (CC\text{-}sial)}$ | 9 | $(Gal\text{-}GlcNAc\text{-}Man)_2ManGlcNAc_2$ | 200±22; n=11 (180-240) | - |

**Figure 1.**

L1 proteins. (A) Schematic representation of membrane-bound L1. (B) SDS-PAGE analysis of L1 constructs. (B) Denaturing IEF gel of L1 constructs. Standard proteins with pI values between 4.45 and 9.6 are shown in the right lane. (D) Summary of the properties of the different L1 samples used for cryoET of adhering liposomes. Each protein is listed along with the number of potential N-linked glycosylation sites it contains, the assumed structure of its N-linked carbohydrates (Elbein et al., 1990; Marchal et al., 2001; Tomiya et al., 2003; Varki, 2007), and structural features of the adhesion interfaces it formed in tomograms. Values in the membrane distance column refer to the mean and standard deviation for n measurements. The minimum and maximum intermembrane distances observed are shown in parentheses.

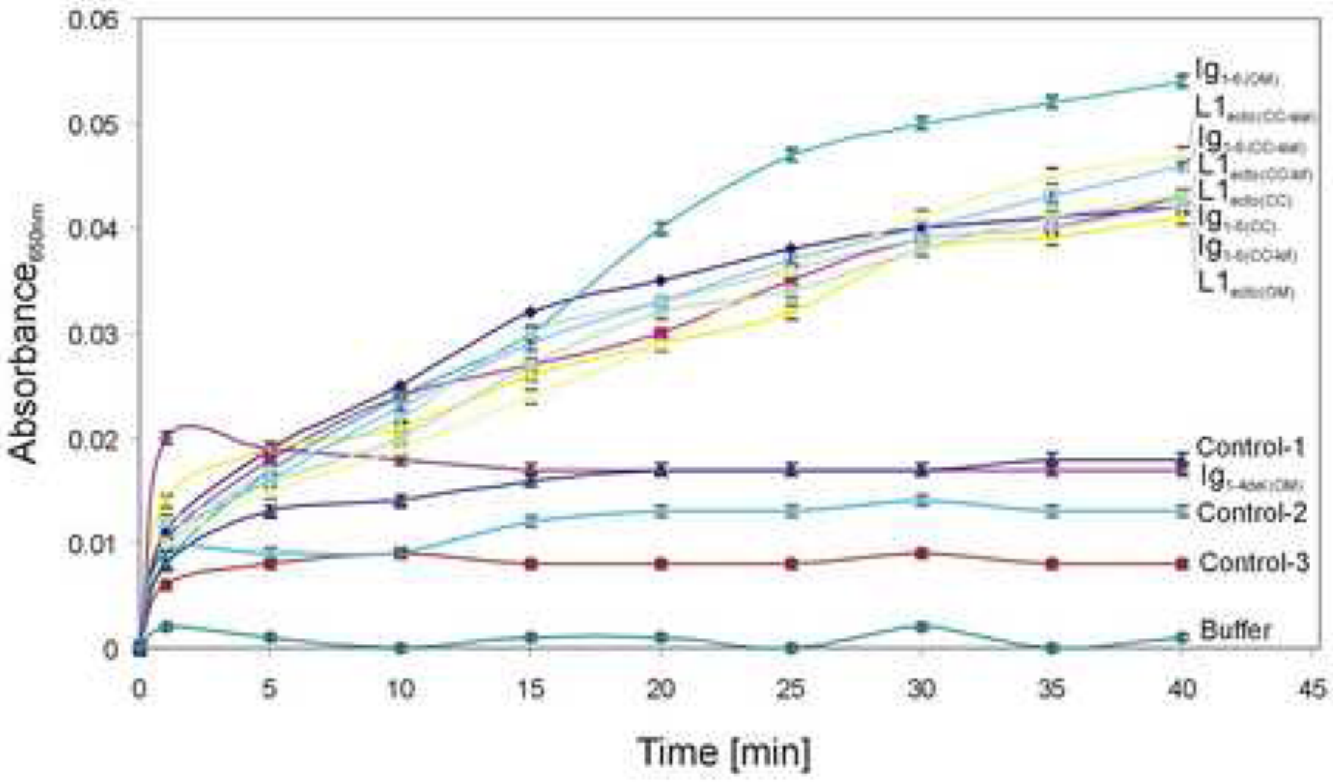


**Figure 2.**

Liposome aggregation assay using different L1 protein constructs. Control-1, -2, and -3 refer to three different His-tagged control proteins (see Experimental Procedures) that did not mediate adhesion when attached to liposomes.

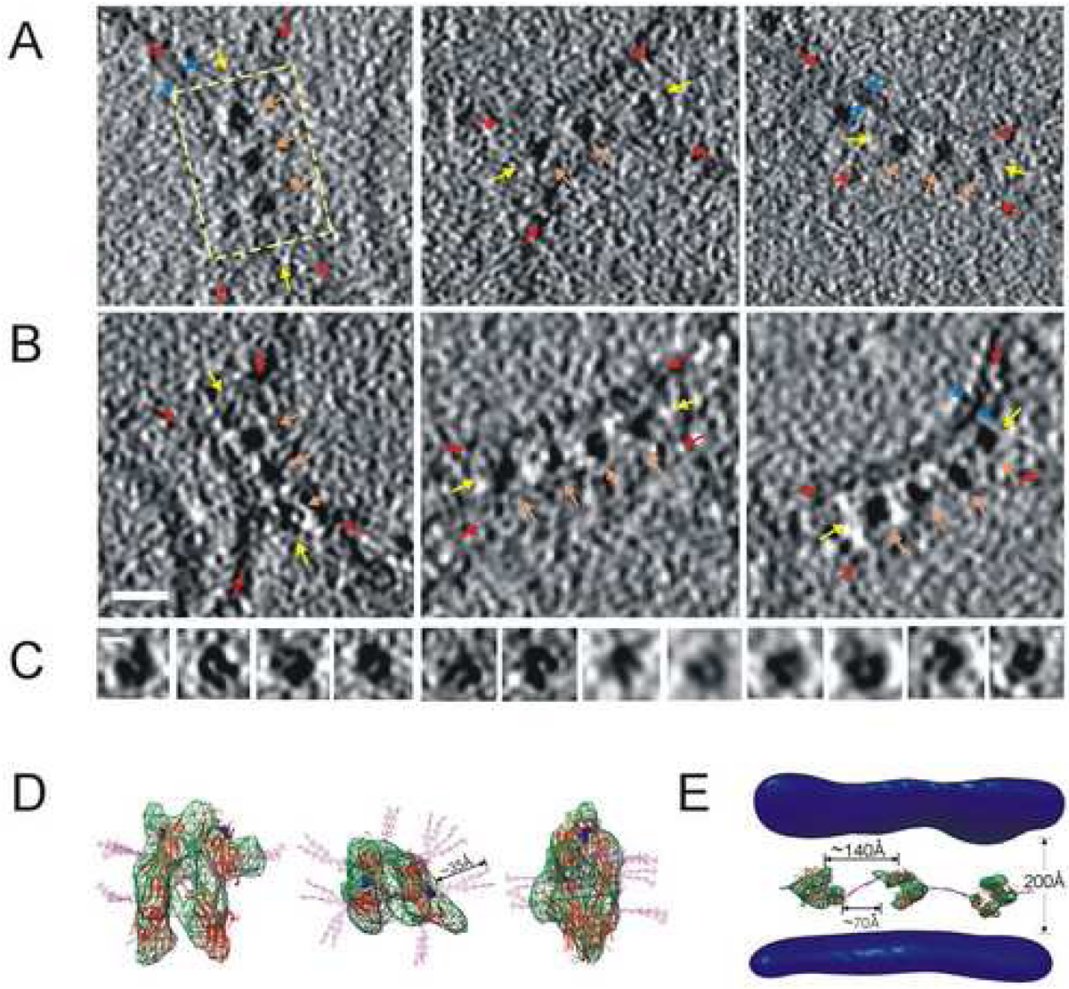


**Figure 3.**

Adhesion interfaces between liposomes prepared with L1 proteins produced in insect cells. (A,B) Tomographic slices (13.6 nm) derived from $L1_{ecto\ (OM)}$ (panel A) and $Ig_{1–6\ (OM)}$ (panel B) samples showing dots (brown arrows) formed at the interfaces (yellow arrows) between neighboring membranes (red arrows). The two leaflets of the membrane bilayer are indicated by blue arrows when apparent. Differences in visibility of the membranes and membrane leaflets may be due to their orientation (strictly perpendicular or at another angle) within the slice. Bar = 20 nm. (C) Gallery of U-shaped dots derived from $L1_{ecto\ (OM)}$ (left six) and $Ig_{1–6\ (OM)}$ (right six) samples. Bar = 5 nm. (D) Side (left, right) and top (middle) views of a Dscam/axonin-1 horseshoe pair (red ribbons) (see Experimental Procedures) fit into a U-shaped adhesion dot density (green; corresponding to the middle dot in panel E). Complex carbohydrates (pink) (derived from pdb code 1w8t) were attached to the predicted locations in two L1 horseshoes for the eight potential N-linked glycosylation sites. Residue Arg184 (highlighted in blue) is located on the outer surface of the adhesion pair. This panel corresponds to Supplementary Movie S2. (E) Horseshoe pairs fit into the densities for three adhesion dots (yellow box in panel A). One carbohydrate from each horseshoe (pink or purple) is shown to demonstrate how carbohydrate-carbohydrate interactions between neighboring horseshoe pairs (totaling ~70 Å for two carbohydrate units) could result in a ~140 Å lateral separation. This panel corresponds to Supplementary Movie S3.

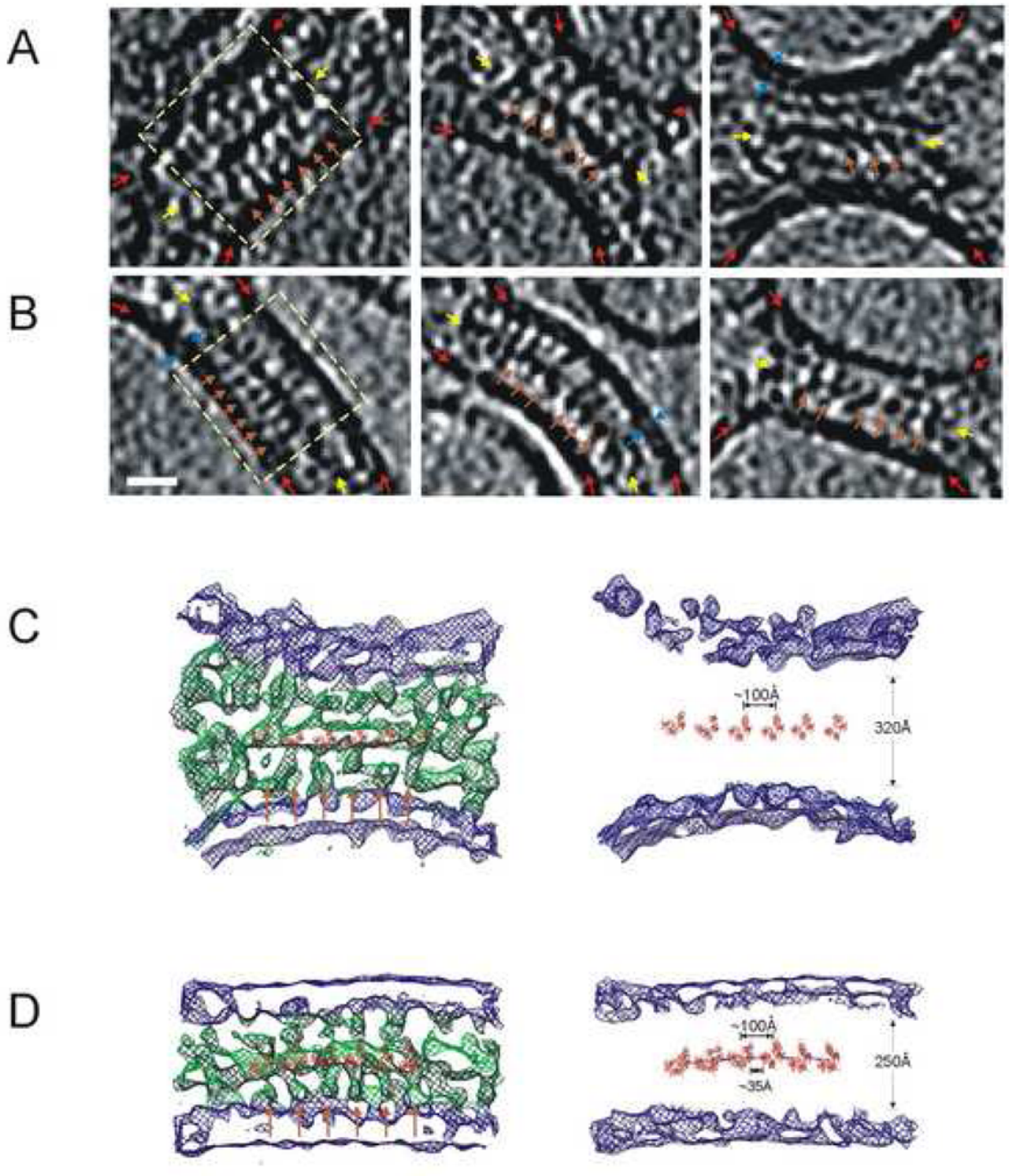


**Figure 4.**

Adhesion interfaces between liposomes prepared with L1 proteins produced in mammalian cells. Brown arrows mark regularly-spaced elongated densities in all panels. The two leaflets of the membrane bilayer are indicated by blue arrows when apparent. (A,B) Tomographic slices (13.6 nm) derived from $L1_{ecto\ (CC)}$ (panel A) and $Ig_{1–6\ (CC)}$ (panel B) samples showing the regular pattern at the interfaces (yellow arrows) formed between neighboring membranes (red arrows). One of the adhesion dots is enclosed in brown circle in the middle image of panel B. Bar = 20 nm. (C,D) Six pairs of interacting horseshoes (modeled using the Dscam/axonin-1 model described in Experimental Procedures) placed into densities. Models were placed to relate the size and spacing of the dots to the paired horseshoe structure rather than to indicate

specific orientations. The densities in panels C and D correspond to the yellow boxes in panels A and B, respectively. In panel D, one carbohydrate (purple) extending ~35 Å from each horseshoe is shown to demonstrate how carbohydrate-protein interactions between neighboring horseshoe pairs could result in a ~100 Å separation. This panel corresponds to Supplementary Movie S4.

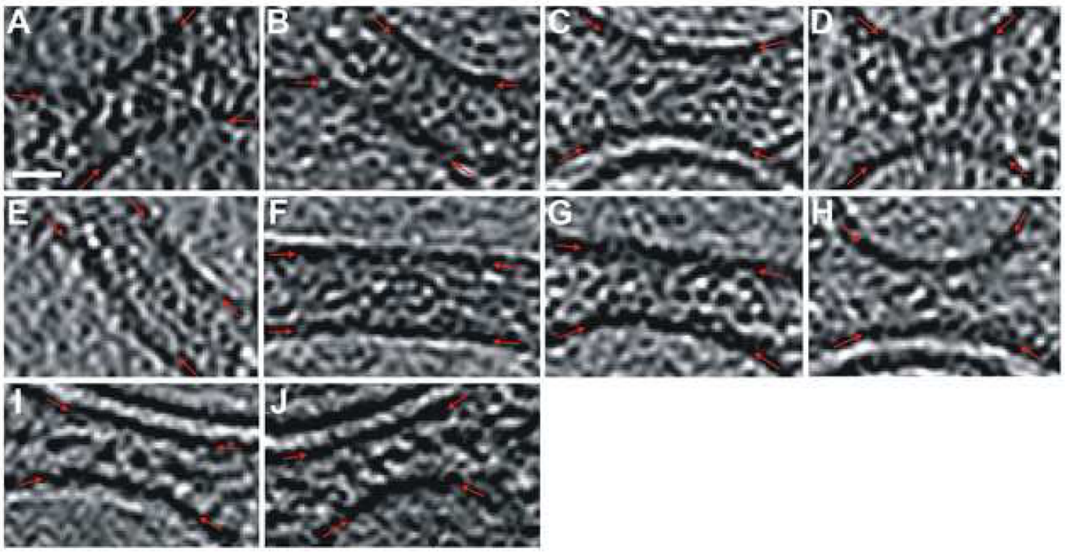


**Figure 5.**

Adhesion interfaces derived from liposomes prepared with mammalian cell-derived L1 proteins with altered carbohydrates. Tomographic slices (13.6 nm) derived from $L1_{ecto\ (CC\text{-}kif)}$ (panels A,B), $L1_{ecto\ (CC\text{-}sial)}$ (panels C,D), $Ig_{1–6\ (CC\text{-}kif)}$ (panels E,F), $Ig_{1–6\ (CC\text{-}sial)}$ (panels G,H), and L1-$R184Q_{ecto\ (CC)}$ (panels I,J). Bar = 20 nm. Neighboring membranes are indicated by red arrows. The lack of a regular pattern in the kifunensine-and sialidase-treated samples is not unexpected given that the carbohydrates in these samples differed from both their untreated counterparts and from the oligomannose structures attached by insect cells, and neither the inhibitor nor the enzyme are likely to be 100% efficient.

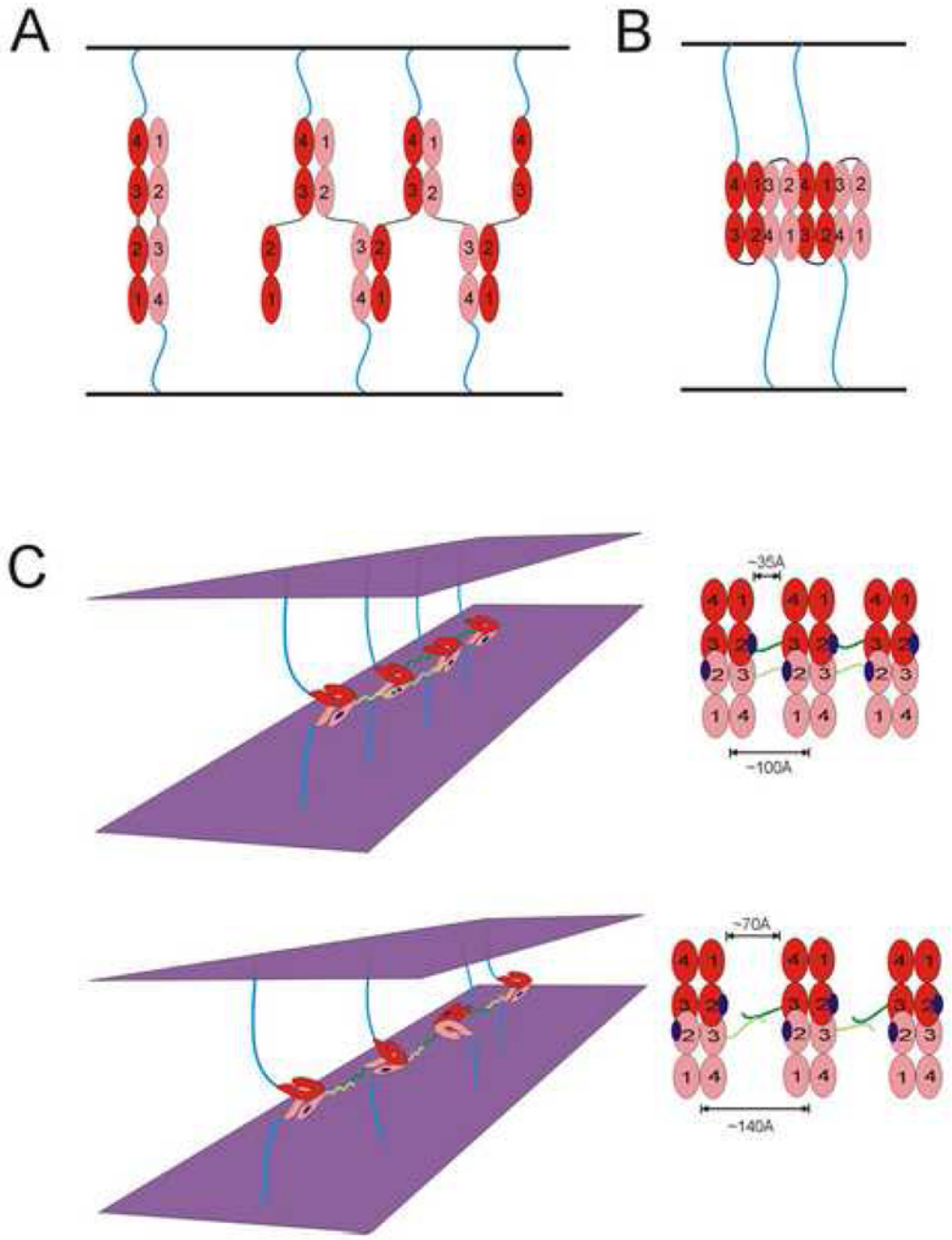


**Figure 6.**

Models for homophilic adhesion. (A) Domain-swapping models for homophilic adhesion (left: domain-swapped dimer; right: domain-swapped multimer) suggested by the structure of hemolin (Su et al., 1998). (B) Zipper model for homophilic adhesion based on the packing of unglycosylated axonin-1 horseshoes in crystals (Freigang et al., 2000). (C) Model for homophilic adhesion mediated by L1 and related proteins suggested by cryo-ET. The horseshoe heads (red and pink) of L1 proteins from adjacent membranes (purple) form *trans* pairs at the adhesion interface, with the lateral separation between pairs being controlled by *cis* interactions mediated by carbohydrates (green). Top: Model for homophilic adhesion for L1 proteins containing complex carbohydrates with terminal sialic acids. Sialic acids on carbohydrates

from one horseshoe interact with a positive patch (blue) on a neighboring horseshoe to create closely and approximately regularly spaced horseshoe pairs. Bottom: Model for homophilic adhesion for L1 proteins containing uncharged oligomannose carbohydrates. Carbohydrate-carbohydrate interactions between uncharged carbohydrates create a “shield” around each horseshoe (see Figure 3D; for clarity, only one carbohydrate per horseshoe is shown in the Figure 6C schematic), resulting in approximately regularly spaced, but randomly oriented, pairs of horseshoes.